ELSEVIER

Chemical Engineering Journal 87 (2002) 301–311

Chemical Engineering Journal

www.elsevier.com/locate/cej

CFD analysis of spinning cone columns: prediction of unsteady gas flow and pressure drop in a dry column

S.V. Makarytchev, T.A.G. Langrish*, D.F. Fletcher

Department of Chemical Engineering, University of Sydney, NSW 2006, Sydney, Australia

Received 12 March 2001; received in revised form 3 August 2001; accepted 10 September 2001

Abstract

Computational fluid dynamics (CFD) simulations have been carried out on the gas flow patterns and pressure distribution in a laboratory-scale (0.15 m diameter) spinning cone distillation column (SCC) in the absence of liquid flow. These simulations show that the flow becomes unstable at a hydraulic Reynolds number (Re^{hyd}, based on the minimum passage size between the cones) above a critical value of about 100. The instability leads to high-frequency oscillations of the velocity components and pressure about their mean values. The discrete nature of the pulsation spectrum indicates that the flow regime is an unsteady laminar one for the small-scale SCC considered here, not a turbulent one. This unsteady regime occurs across the entire range of the column operation ($200 < Re^{hyd} < 2000$). The instability develops regardless of whether the inner cone is rotating (as in normal operation) or not. For normal (rotating) operation, the pulsations are synchronised with the rotor motion. Comparison of time-average pressure values with experiment shows that the actual pressure drop through the column stage is predicted by the CFD model to within 10–15%. The pressure pulsations are likely to cause mechanical vibrations and are a consequence of the flow instability.

Keywords: Computational fluid dynamics; Spinning cone distillation column; Pulsations

1. Introduction

The spinning cone distillation column (SCC) is a distillation device used in the food industry for the separation of volatile components from liquids and slurries. An SCC consists of a vertical succession of alternate rotating and stationary cones (Fig. 1). Liquid flows as a film down the stationary cone, drains into the base of the rotating cone, and moves upward on the rotating cone, again as a film, by the action of centrifugal force. Gas flows up the column countercurrent to the flow of the liquid. Mass transfer from the liquid to the vapour phase in an SCC takes place through the large surface area of the film, which may be very thin (less than 1 mm) of liquid spread out on the spinning cones and through the liquid spray in the regions between spinning and stationary cones. There may be several dozen cone sets (stages) in a commercial column. An essential feature of the columns is the presence of fins attached to the lower surfaces of spinning cones. The fins act as a centrifugal pump to an extent, adding to the gas pressure drop along the column and giving some additional control of pressure along the column. The number and design of the fins affect the pressure distribution within the column and are important for effective gas–liquid separation. Pressure control is important in the processing of thermally sensitive materials that are commonly processed in this type of equipment, since these are frequently separated under vacuum to keep temperatures low, and the temperatures are directly linked to the operating pressures.

Until recently, the design of spinning cone columns has largely been based on empirically established procedures and correlations [11,12]. However, expanding commercial applications mean that a more fundamental understanding of the physical processes involved is necessary to give a more rigorous approach to column design and operation. The hydrodynamic regimes and the spatial structure of the liquid film flow over a rotating cone surface have already been studied [1,6], and we have developed correlations for the thickness and the average velocity of the wavy liquid film on such surfaces [7].

In this work, we consider the hydrodynamics of the gas flow in the absence of liquid flow. In particular, we are interested in the gas flow regime and the pressure drop through the column, which has the practical significance of being an approximation to the actual situation in an SCC for small liquid loads. To address the complex internal geometry of

* Corresponding author. Tel.: +61-2-9351-4568; fax: +61-2-9351-2854.
E-mail address: timl@chem.eng.usyd.edu.au (T.A.G. Langrish).

1385-8947/02/$ – see front matter
PII: S1385-8947(01)00245-5

Nomenclature

A_{inlet}	inlet area (m^2)
P	pressure (Pa)
Q	volumetric flow rate ($m^3\,s^{-1}$ or l/min)
R_H	width of the passage between cones in SCC (m)
R_{FI}	inner radius of the fixed cone (m)
R_{SO}	outer radius of the spinning cone (m)
Re^{hyd}	hydraulic Reynolds number defined by Eq. (1)
Re^{rot}	rotational Reynolds number defined by Eq. (2)
U_{inlet}	inlet velocity ($m\,s^{-1}$)
V	characteristic velocity, as defined ($m\,s^{-1}$)
V_{column}	volume of the column (m^3)

Greek letters

ν	kinematic viscosity ($m^2\,s^{-1}$)
τ_{res}	residence time of the gas in the column (s)
τ_{rot}	characteristic time of rotation (s)
ω_{rotor}	angular velocity of the rotor motion (s^{-1} or rpm)
Ω	angular velocity of the system of coordinates (s^{-1} or rpm)

the column, we use a computational fluid dynamic (CFD) approach to analyse the fluid flows. Use of CFD analysis is particularly necessary due to the presence of fins, the number and design of which affect the topology of the CFD model and the computational approach used (rotating coordinates). The base-case CFD model for gas-only flow in SCCs described here will be developed further to analyse the more complex gas–liquid (two-phase) flows, as a basis for future optimisation of SCC design and operation.

Previous measurements, CFD modelling and CFD analysis of flow patterns has been carried out for conventional distillation column trays [5,10,16]. Wagenaar et al. [15] modelled and measured particle dynamics and gas-phase flow in a rotating cone reactor, with the gas flow being treated with a boundary layer approximation. They commented that "*A more accurate description of the flow behaviour of the gas phase can be obtained if a computational fluid dynamics* (*CFD*) *model is applied*." Such a CFD analysis is reported in this work for this equipment, which is novel because it involves strongly swirling, transitional flows.

2. Geometry and computational approach

2.1. The modelled equipment

A laboratory-scale SCC, for which detailed experimental data (pressure drop, flooding characteristics and mass-transfer coefficients) are available, has been described by [14], and this has been used as the basis for the CFD geometry. The geometric parameters for this column are given in Table 1, and the notation used is illustrated in Fig. 2. In this forty-stage SCC, the vertical position of the shaft can be altered, thus affecting the distance between the fixed and the spinning cones and the topology of the CFD model.

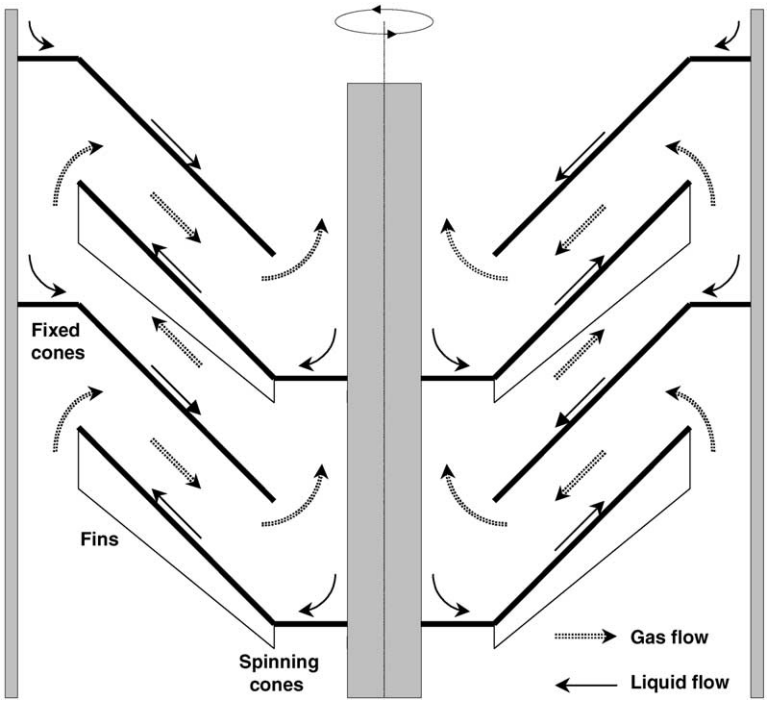

Fig. 1. A section through part of an SCC.

Table 1
Parameters of the modelled SCC

Parameter	Value
Spinning cone	
Inner radius, R_{SI} (m)	0.025
Outer radius, R_{SO} (m)	0.064
Inner fin depth, d_{FI} (m)	0.004
Outer fin depth, d_{FO} (m)	0.007
Number of fins	3
Fixed cone	
Inner radius, R_{FI} (m)	0.035
Outer radius, R_{FO} (m)	0.074
Column	
Shell inner radius, R_C (m)	0.074
Shaft radius, R_S (m)	0.021
Cone pitch, P_C (m)	0.021
Cone angle, θ (°)	50
Number of cone sets	40

2.2. The CFD model—numerical considerations

The simulations used the CFD program CFX4.3™, which uses a structured mesh and a finite volume formulation to discretise the Navier–Stokes equations. These equations describe the fluid flows in this equipment and comprise equations for conservation of mass and momentum in this isothermal situation. Full details of the equations and the numerical scheme are given in the User Manual [2]. A discussion of various convection schemes is given in [13]. This study showed that the high order schemes implemented in CFX4.3 could reproduce the swirl flow velocity fields obtained using orthogonal grids aligned with the flow using non-orthogonal, non-flow aligned grids. The Van Leer limiter (see [3]) was implemented for all the velocity components. This scheme is second-order accurate and maintains monotonicity across computational cells, hence preventing numerical oscillations in the solution domain. The SIMPLEC algorithm [9] was used for pressure correction. The working fluid was chosen as incompressible and Newtonian. As a convergence criterion, the sum of the absolute mass source residuals over all cells was less than 0.1% of the total flowrate. This resulted in a sufficient number of iterations being carried out for each time step so that changes in monitoring point values were not discernible with further iterations. The variation of residual values with iterations were checked to ensure that the residuals for all the equations were consistently decreasing and approaching their limit of the accuracy for single precision. This minimised the chance of error accumulation over successive time steps. No turbulence model was used here, and the unsteady nature of the flow was resolved by transient simulations.

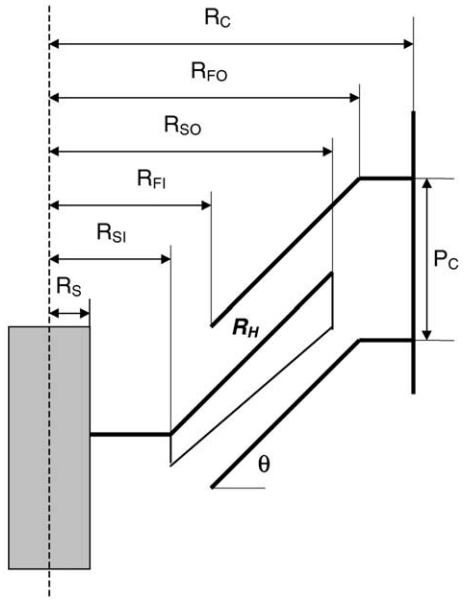

Fig. 2. The geometry of an SCC stage.

2.3. The CFD model—implementation

The number of column stages chosen for the CFD model (three) represents a compromise between model complexity and the ability to resolve flow and pressure fields in the regions far from the entry and exit boundaries. The lower and the upper stages (stages 1 and 3, respectively) exist to give well-developed boundary conditions for the

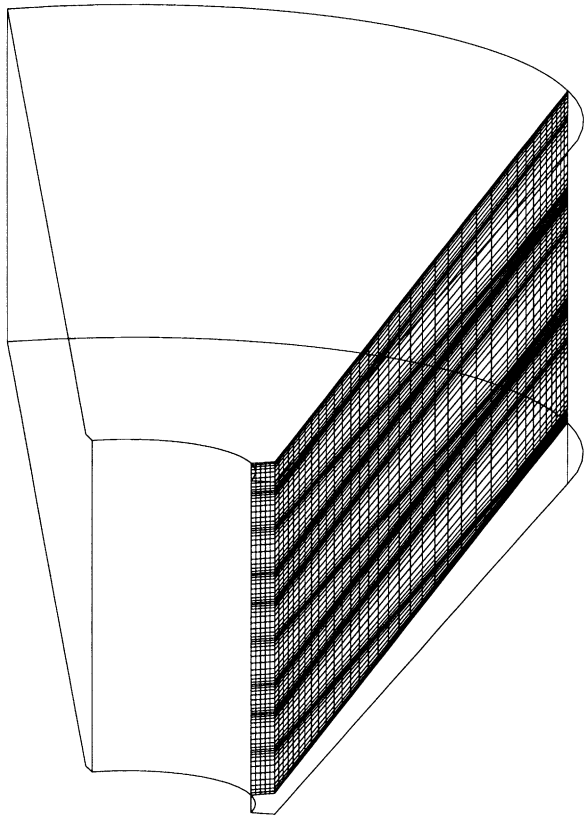

Fig. 3. Model outline and three-dimensional section of the computational grid.

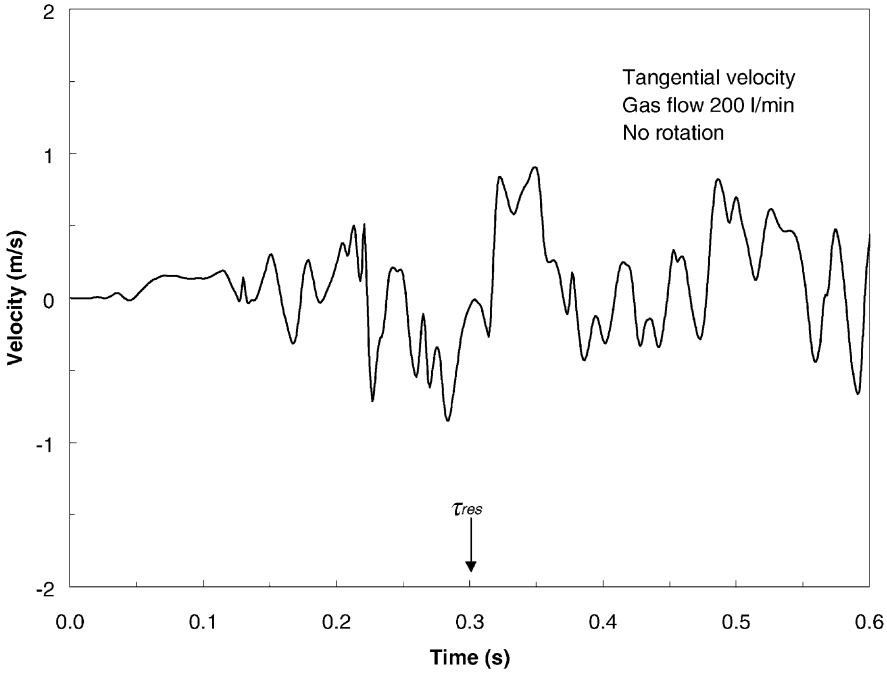

Fig. 4. The onset of the flow instability for no rotation, gas flowrate 200 l/min.

middle stage (stage 2). Two monitoring points, MP1 and MP2, are located in the centres of the stage 2 exit and entry, respectively. Pressure drop is monitored across stage 2, between points MP1 and MP2. The simulations show that the velocity field is the same at the entry and exit of stage 2.

Fig. 3 shows the outline of the model and the vertical cross-section of the three-dimensional computational grid. The grid has 90 axial, 40 radial, and 40 tangential cells. In the tangential direction, the model is a 120° segment of a cylinder with the fins at the 60° plane and the periodic boundaries at its sides.

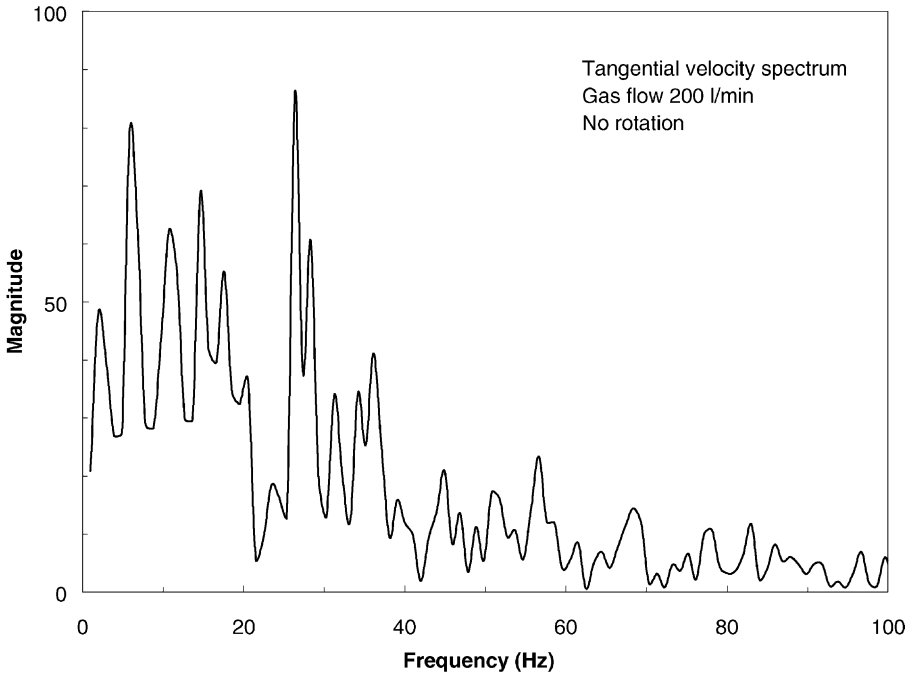

Fig. 5. The spectrum of the velocity pulsation with no rotation, gas flowrate 200 l/min.

2.4. Boundary conditions

Different conditions were applied to the five groups of surfaces: gas entry (opening of the column between the lip of the lowest fixed cone and the shaft); gas exit (opening of the column between the lip of the upper fixed cone and the shaft); rotor (surfaces of the column shaft, the spinning cones, and the fins); stator (surfaces of the fixed cones and the outer shell of the column); periodic boundaries (surfaces at the 0 and 120° planes of the model segment). The conditions were:

- Gas entry: inlet boundary with the normal velocity determined by the volumetric flowrate of gas through the column, $U_{\text{inlet}} = Q/A_{\text{inlet}}$. For example, $Q = 200\,\text{l/min}$ and $A_{\text{inlet}} = 0.0035\,\text{m}^2$ gives a normal inlet velocity of $U_{\text{inlet}} = 0.952\,\text{m s}^{-1}$.
- Gas exit: pressure boundary with the pressure value set to zero, $P_{\text{exit}} = 0$.
- Rotor: due to the geometrical complexity of the rotor (presence of fins), the calculations have been made in coordinates rotating with the angular velocity equal to that of the rotor, $\Omega = \omega_{\text{rotor}}$. The rotor is then stationary in a rotating frame of reference, and no special boundary conditions were applied here.
- Stator: this rotates with an angular velocity opposite to that of a rotor, $\omega_{\text{stator}} = -\Omega$. Therefore, the fixed cones and the outer shell of the column are counter-rotating walls in rotating coordinates.

2.5. The solution

Both the processing of the model topology and grid and the solution of the conservation equations for mass and momentum have been carried out using the commercial flow modelling package CFX4.3™, as described earlier. With the $30 \times 40 \times 40$ cells per stage grid shown in Fig. 3, the solution speed on a DEC Personal Workstation 500 is about 400 iterations per hour. It then takes less than an hour for a well-converged steady-state solution (at low Reynolds numbers), and up to several days for a sufficiently long transient run (~0.1 physical second per day of computation). The predicted pressure drop was found to be mesh-independent within 10% compared with the use of a grid as coarse as $18 \times 24 \times 24$ cells per column stage. The time step used was 0.1 ms for most of the simulations for which typically 10 iterations per time step were required to reduce the residual to the required value. Note that this time step is much smaller than that required to resolve the frequency spectra.

3. Flow regime

3.1. Reynolds numbers

The hydrodynamic regime of the flow is characterised by the Reynolds numbers. Those related to this flow situation are: (i) a "hydraulic" Reynolds number, Re^{hyd}, for a flow in a duct, based on a hydraulic radius R_{H} (in SCC, the minimum width of passage between the cones, Fig. 2):

$$Re^{\text{hyd}} = \frac{VR_{\text{H}}}{\nu} = \frac{Q}{2\pi R_{\text{FI}}\nu}, \tag{1}$$

(ii) a "rotational" Reynolds number, Re^{rot}, for an unbounded fluid flow over a rotating disk:

$$Re^{\text{rot}} = \frac{\omega_{\text{rotor}} R^2}{\nu} = \frac{\omega_{\text{rotor}} R_{\text{SO}}^2}{\nu}. \tag{2}$$

These estimates are upper values—the Reynolds number is less elsewhere in the SCC, since the radius in Eq. (1) is the smallest physical value, and that in Eq. (2) is the largest physical value.

For the ideal cases of the straight pipe and the rotating disk, the onset of the first instability and of fully developed

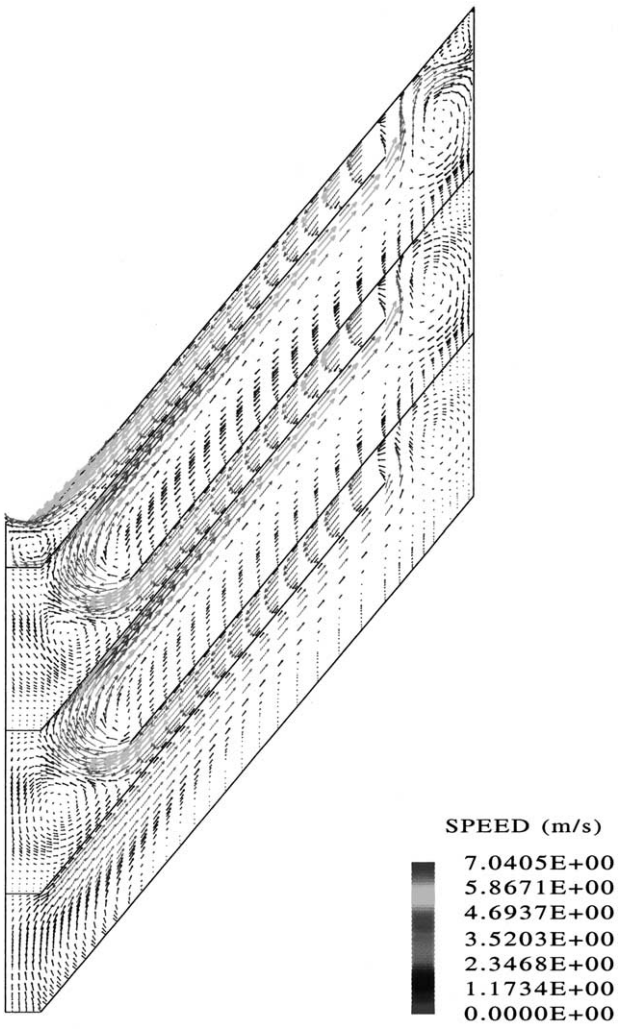

Fig. 6. A snapshot of the flow pattern for no rotation, gas flowrate 200 l/min.

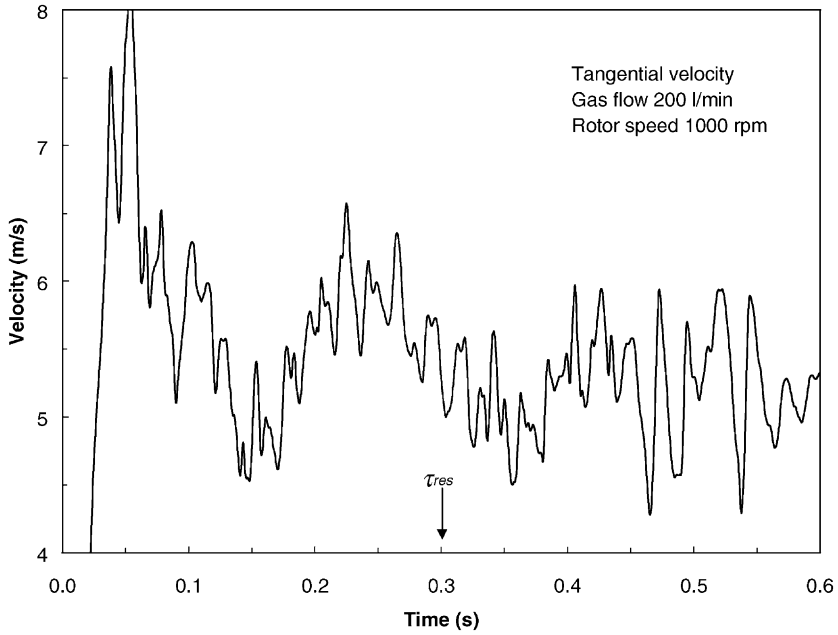

Fig. 7. Velocity pulsation at 1000 rpm, gas flowrate 200 l/min.

turbulence is characterised by the following critical values of these numbers [4,8]:

Flow regime	Unstable	Fully turbulent
Re^{hyd}	>2000	>3000 (pipe)
Re^{rot}	$>0.9\times10^5$	$>3.2\times10^5$ (disk)

Table 2 shows the range of the column operating conditions and the corresponding ranges of the Reynolds numbers

Table 2
The operating conditions for this SCC

Parameter	Value
Flowrate of gas, Q (l/min)	40–400
Hydraulic Reynolds number, Re^{hyd}	202–2020
Rotational speed, ω (rpm)	500–1500
Rotational Reynolds number, Re^{rot}	$(0.14–0.43)\times10^5$

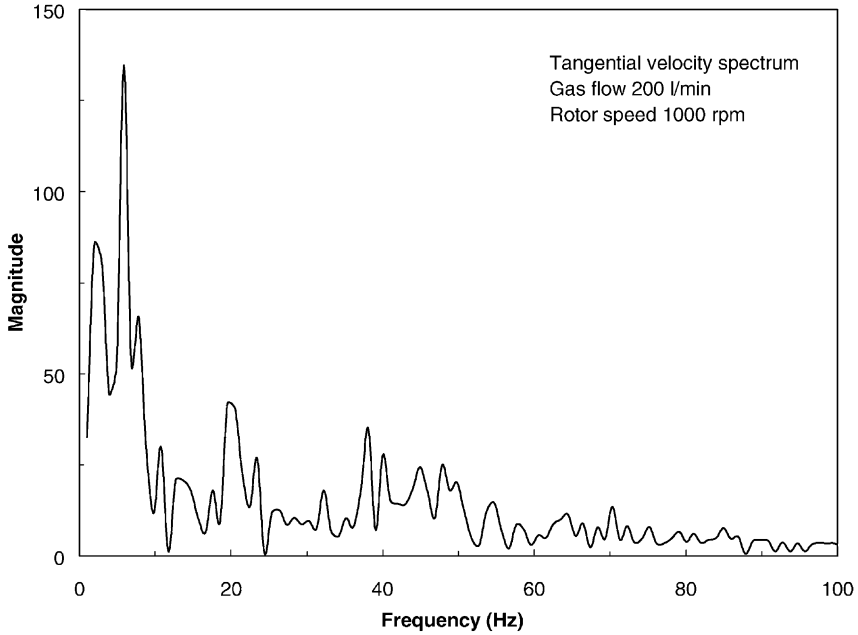

Fig. 8. Spectrum of velocity pulsation at 1000 rpm, gas flowrate 200 l/min.

in this case. Since the ranges of both the Reynolds numbers are below the critical values for pipes and disks, the gas flow may be expected to be laminar. In respect to Re^{hyd}, the flow would become increasingly prone to instability when the gas flowrate approaches its critical value of ∼400 l/min. In relation to rotation, the flow may be expected to be stable up to a rotational speed of about 3000 rpm, which is beyond the normal range of operation. However, the above stability criteria are for ideal cases of straight pipe and unbounded rotating geometries. The actual stability of the flow in equipment as complex as SCCs must be investigated. This necessitates the use of transient calculations.

3.2. Steady sub-critical flow

These simulations show that the steady-state flow regime in this SCC exists only at very low gas flowrates. In the absence of rotation, the critical Reynolds number for the onset of the first instability has been found to be as low as $Re^{hyd}_{crit} = 100 (Q = 20\,l/min)$. The steady-state flow pattern at $Re^{hyd} < Re^{hyd}_{crit}$ is characterised by the absence of recirculation zones and complete axial symmetry. The maximum values of the velocity and pressure gradients coincide with the minimum flow area between the rotating and the stationary cones. This steady-state regime, however, is of little practical relevance since it only occurs below the range of typical SCC operating conditions.

3.3. Unsteady flow

At values of Re^{hyd} above the critical value of 100, the flow becomes unstable. Fig. 4 shows the development of the instability at $Re^{hyd} = 1000 (Q = 200\,l/min)$ after initiating the flow, in the form of a temporal profile of the tangential velocity component at the monitoring point at the exit of the second section. Flow pulsations develop after a period of about one residence time ($\tau_{res} = Q/V_{column}$). The spectrum of established velocity pulsation at $\tau > \tau_{res}$ is shown in Fig. 5. The spectra for this and other velocity components are discrete. The multiplicity of the modes of pulsation reflects the geometric complexity of the model, since there are many length scales within the column stage. The discrete nature of the spectra suggests that this behaviour reflects a flow instability and not fully developed turbulence, because turbulence would be characterised by continuous power spectrum across a range of frequencies. It is worth noting that, at present, there are no developed turbulence models for transitional flows. The low Reynolds number models available are actually high Reynolds number models that allow integration of the turbulence equations to the wall.

The unsteady flow pattern differs from the steady one. It is characterised by the presence of multiple eddies (recirculation zones) in the corners of the inner and outer throat and even between the cones at higher flowrates (Fig. 6). The maximum values of velocity are now located underneath the rotating cone. The pressure drop is largest in the inner throat region of the column where the changes of velocity direction and magnitude are most significant.

To investigate these pulsations in more detail, several snapshots of the flow field at time intervals of 0.1 s have been plotted. Investigation of the results has shown that, while the macroscopic structure of the flow field is basically preserved, the pulsations correspond to small chaotic displacements of the flow streamlines, formation and disappearance of additional eddies, and other irregularities of the flow pattern. The most significant disturbances occur in the inner and the outer throat regions, where the flow changes its direction. These frequent changes of the flow direction and area are reasons for the inherent flow instability and the lower value of the critical Reynolds number for gas flow in SCCs (∼100) compared with that for pipe flows (∼2000).

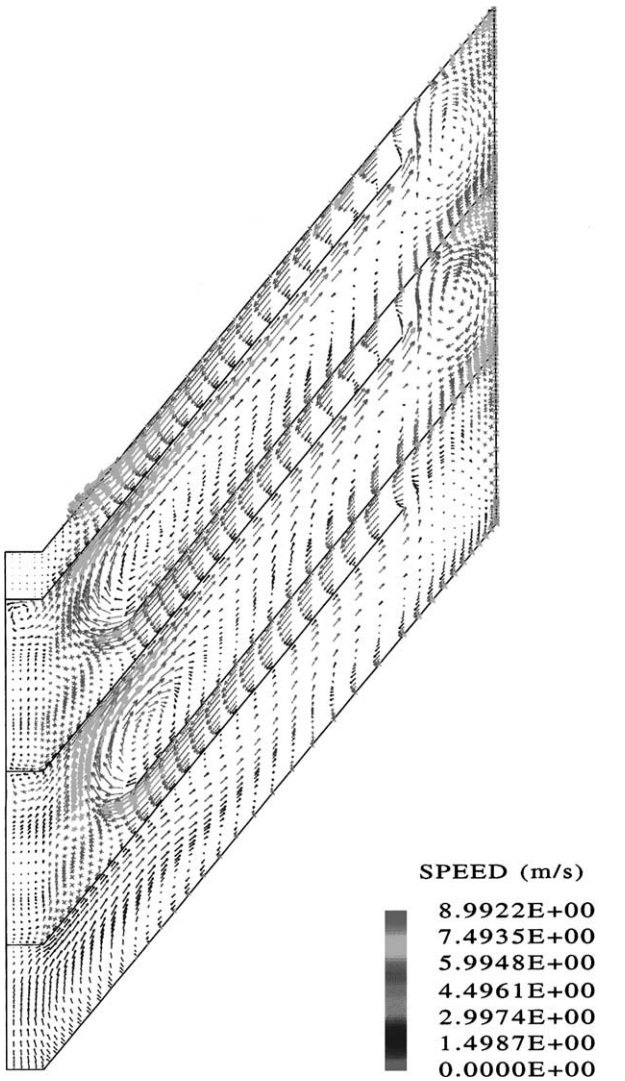

Fig. 9. Vertical section of the flow pattern at 1000 rpm, gas flowrate 200 l/min.

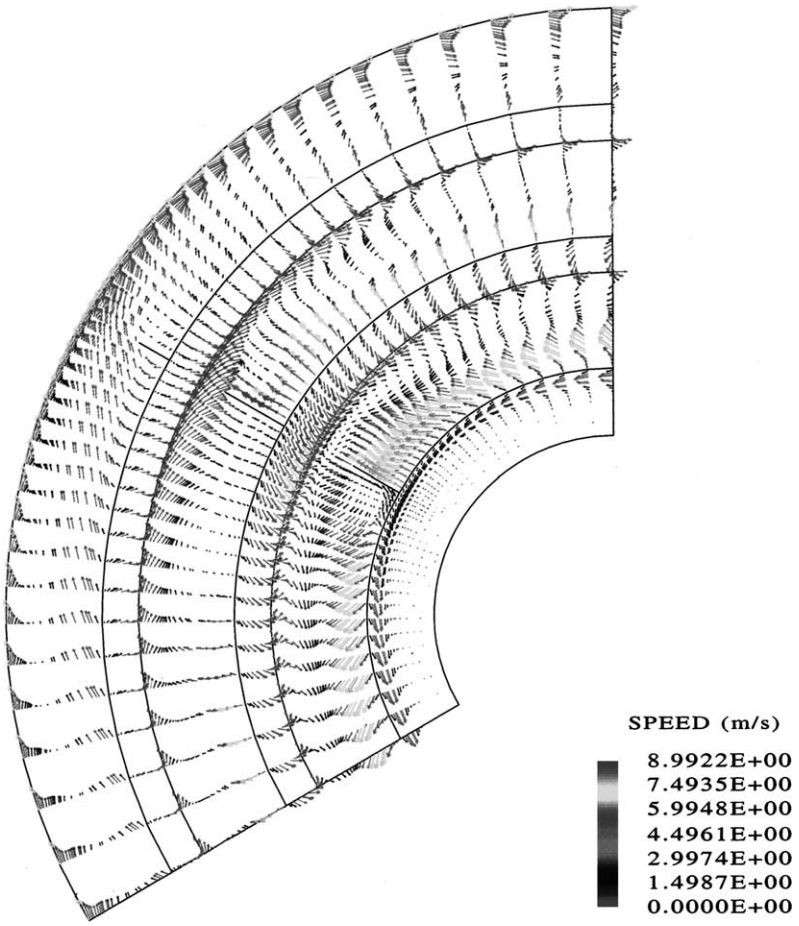

Fig. 10. Horizontal section of the flow pattern at 1000 rpm, gas flowrate 200 l/min (note the velocities are shown in the rotating frame).

3.4. Effect of rotation

Adding rotation affects both the character of the pulsations and the flow pattern. A transient record of the velocity at a rotor speed of 1000 rpm is shown in Fig. 7. Instabilities now develop faster than in the no-rotation case, at $\tau > \tau_{\text{rot}} = (\omega_{\text{rotor}})^{-1}$. These instabilities are forced oscillations in an already unstable flow system driven by the rotor motion. The spectrum of pulsation (Fig. 8) is simpler than that for the case of no rotation, since the presence of regular motion removes some of the spectral lines and decreases the magnitude of others. The frequency of fins passing a fixed spatial point ($3 \times \omega_{\text{rotor}}$) is always present in the spectrum. At higher rotational speeds this frequency becomes the dominant mode of oscillation. Changing the rotor speed leads to a corresponding shift of this dominant mode. Thus there is a clear effect of synchronisation of the flow pulsation by the rotor motion.

An overview of the established velocity field at 1000 rpm is shown in Fig. 9. The rotation results in a significant increase of both the velocity and the pressure in the outer throat region. These aspects make the distribution of flow parameters more homogeneous in the radial direction. In the tangential direction, the flow pattern becomes asymmetric. The regions of maximum velocity and pressure gradient are now located in the vicinity of fins (Fig. 10).

4. Pressure drop

4.1. Comparison with experiment

Due to velocity oscillations, the pressure also pulsates, so that time averaging is required for comparison of the pressure drop with experiment. Fig. 11 shows a typical transient record of the pressure at the entry and exit of the middle column stage. Using records of this type, the pressure drop has been calculated as the difference between entry and exit pressure values averaged over a 0.1–0.3 s time interval after a transitional period corresponding to the residence time of gas in the system ($\tau > \tau_{\text{res}}$). The CFD-predicted pressure drops are compared with the measurements in Fig. 12, and the deviation of the pressure drop predictions from the experimental values is also given in Table 3, showing that the pressure drop is predicted by the CFD model to within 10–15% across the entire range of operating conditions.

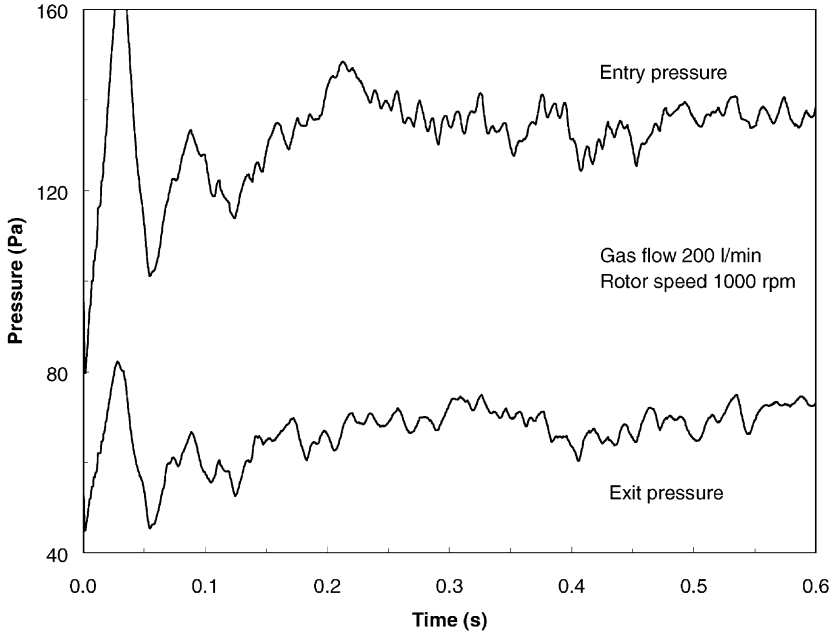

Fig. 11. The pressure at the entry and the exit of the column stage, gas flowrate 200 l/min, 1000 rpm.

Taking into account the pulsating nature of the flow and the fact that the experimental values themselves have a scatter of around 10%, the agreement of the model predictions with measurements is very good.

4.2. Practical implications of pulsations

Under certain operating conditions, pressure pulsations may lead to mechanical vibrations of the column. Due to the

Table 3
Percent deviation of pressure drop prediction from experiment

Air flow (l/min)	Rotor speed (rpm)			
	0	500	1000	1500
100		−7	−5	13
200	−14	−17	0	4
300		−4	10	4

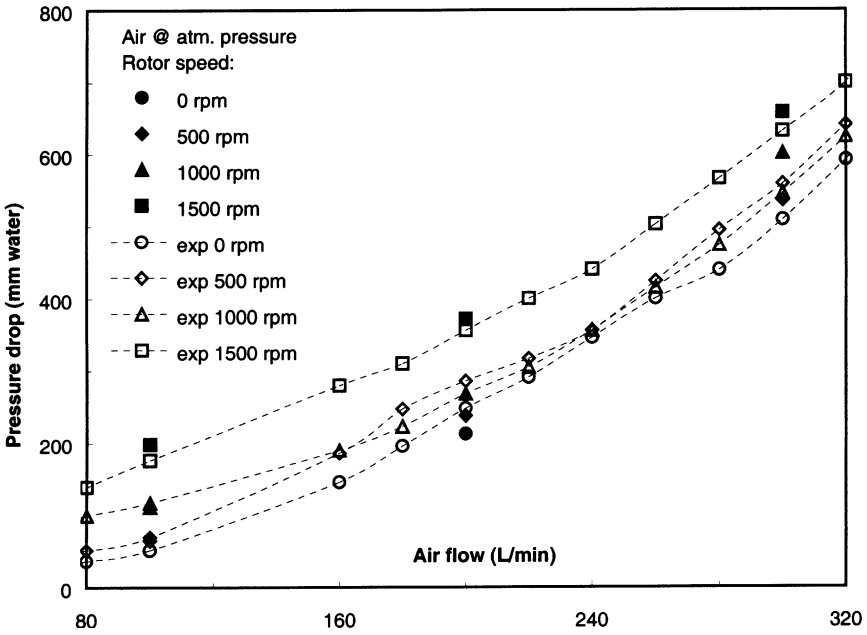

Fig. 12. Comparison of the predicted (black markers) and the measured pressure drops.

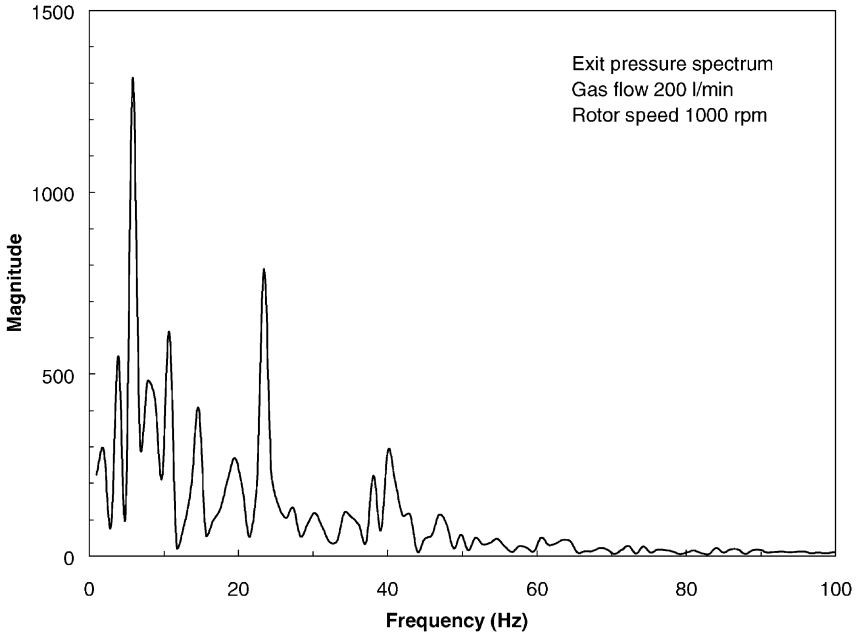

Fig. 13. Spectrum of pressure pulsation, gas flowrate 200 l/min, 1000 rpm.

effect of synchronisation between the rotor motion and the gas flow pulsation, conditions exist for effective energy exchange between the mechanical and the hydrodynamic parts of an overall SCC system. Fig. 13 indicates that significant oscillation power is contained in a low-frequency part of the pressure spectrum even for a three-stage SCC considered in this work. Lower frequencies are possible in a multi-stage (say, forty-stage) SCC. These low frequencies, or their harmonics, may resonate with the mechanical modes of oscillation and excite, for instance, waves propagating up and down along the axis of the column. Thus the mechanical and overall stability of the column operation becomes of practical concern.

Hydrodynamic causes of vibration (flow pulsation) may be significantly reduced or even entirely eliminated by the changes in gas passage design and/or operating parameters of the column. Exploration of the design and operation alternatives may only be done by using a model that reflects the detailed geometry of the equipment of interest. The CFD approach to SCC analysis and the computational model of the column being developed in this work are capable of such development and optimisation tasks. However, development of the approach to include two-phase flow is necessary before such tasks can be carried out for this system, and such a development will be carried out in future work.

5. Conclusions

1. The gas flow in an SCC under conditions of practical interest ($Re^{hyd} > 100$) is unstable. The instability is manifested as pulsations of the velocity components and pressure around their average values. Spectral analysis of these pulsations indicates that the regime of the flow is an unsteady laminar one, but not fully developed turbulence. This regime occurs across the entire range of operation for the SCC considered ($200 < Re^{hyd} < 2000$).
2. Time-averaged values of the CFD-predicted pressure drops agree with experiment within 10–15% over the whole range of column operating conditions.
3. Pressure pulsations may lead to mechanical vibrations in the equipment and instability of the column operation at small liquid loads.

Acknowledgements

This work has been supported by an Australian Research Council Large Grant.

References

[1] O. Al-Hawaj, A numerical study of the hydrodynamics of a falling liquid film on the internal surface of a downward tapered cone, Chem. Eng. J. 75 (3) (1999) 177–182.
[2] CFX 4, Solver Manual, CFX International, AEA Technology, Harwell, Didcot, Oxon, 1997.
[3] C. Hirsch, Numerical Computation of Internal and External Flows, Vol. 2, Wiley, New York, 1990, pp. 536–545.
[4] Kobayashi, Review: laminar-to-turbulent transition of three-dimensional boundary layers on rotating bodies, Trans. ASME 116 (1994) 200–211.
[5] C.J. Liu, X.G. Yuan, K.T. Yu, X.J. Zhu, Fluid-dynamic model for flow pattern on a distillation tray, Chem. Eng. Sci. 55 (12) (2000) 2287–2294.

[6] S.V. Makarytchev, T.A.G. Langrish, R.G.H. Prince, Structure and regimes of liquid film flow in spinning cone columns, Chem. Eng. Sci. 53 (8) (1998) 1541–1550.
[7] S.V. Makarytchev, T.A.G. Langrish, R.G.H. Prince, Thickness and velocity of wavy liquid films on rotating conical surfaces, Chem. Eng. Sci. 56 (1) (2001) 77–87.
[8] L.F. Moody, N.J. Princeton, Friction factors for pipe flow, Trans. Am. Soc. Mech. Eng. 66 (1944) 671–684.
[9] S.V. Patankar, Numerical Heat Transfer and Fluid Flow, Hemisphere, New York, 1980.
[10] K.E. Porter, K.T. Yu, S. Chambers, M.Q. Zhang, Flow patterns and temperature profiles on a 2.44 m diameter sieve tray, Trans. IChemE Chem. Eng. Res. Des. 70 (5) (1992) 489–500.
[11] R.G.H. Prince, S.Y. Desho, T.A.G. Langrish, Spinning cone column capacity and mass-transfer performance, IChemE Symp. Ser. 142 (1997) 769–781. Proceedings of the Distillation and Absorption '97, Maastricht, The Netherlands.
[12] R.G.H. Prince, T.A.G. Langrish, The spinning cone flavour distillation column: a review, in: Proceedings of the CHEMECA-97, Rotorua, New Zealand, MT1b, 1997.
[13] N.A. Shore, B.S. Haynes, D.F. Fletcher, A.A. Sola, Numerical aspects of swirl flow computations, in: R.L. May, A.K. Easton (Eds.), Proceedings of the Seventh Biennial Conference on Computational Techniques and Applications: CTAC95, Melbourne, July 3–5, 1995, pp. 693–700.
[14] S. Sykes, Operating characteristics of spinning cone columns, Ph.D. Thesis, The University of Sydney, Sydney, Australia, 1995.
[15] B.M. Wagenaar, J.A.M. Kuipers, W.P.M. van Swaaij, Particle dynamics and gas-phase hydrodynamics in a rotating cone reactor, Chem. Eng. Sci. 49 (7) (1994) 927–936.
[16] K.T. Yu, X.G. Yuan, X.Y. You, C.J. Liu, Computational fluid-dynamics and experimental verification of two-phase two-dimensional flow on a sieve column tray, Trans. IChemE Chem. Eng. Res. Des. 77 (6) (1999) 554–560.